Inverse Problems in Engng, 2002, Vol. 10, No. 2, pp. 163–182

Taylor & Francis
Taylor & Francis Group

A BOUNDARY ELEMENT REGULARIZATION METHOD FOR THE BOUNDARY DETERMINATION IN POTENTIAL CORROSION DAMAGE

D. LESNIC[c,*,1], J.R. BERGER[b] and P.A. MARTIN[a]

[a]*Department of Mathematical and Computer Sciences,* [b]*Division of Engineering, Colorado School of Mines, Golden, CO 80401-1887, USA;* [c]*Department of Applied Mathematics, University of Leeds, Leeds, LS2 9JT, UK*

(Received 18 December 2000; In final form 28 December 2001)

In this paper, we consider the inverse problem for the Laplace equation in two-dimensions which requires the determination of the location, size and shape of an unknown, or partially unknown, portion $\gamma \subset \partial\Omega$ of the boundary $\partial\Omega$ of a solution domain $\Omega \subset R^2$ from additional Cauchy data on the remaining portion of the boundary $\Gamma = \partial\Omega - \gamma$. This problem arises in the study of quantitative non-destructive evaluation of corrosion in materials in which boundary measurements of currents and voltages are used to determine the material loss caused by corrosion. This inverse problem is approached using the boundary element method (BEM) in conjunction with the Tikhonov first-order regularization procedure. The choice of the regularization parameter is based on an L-curve type criterion although, alternatively one may use the discrepancy principle. Several examples which involve noisy Cauchy input data are thoroughly investigated showing that the numerical method produces a stable approximate solution which is also convergent to the exact solution as the data errors tend to zero.

Keywords: Boundary determination; Corrosion damage; Boundary element method; Regularization; L-curve

1. INTRODUCTION

The purpose of this work is to demonstrate that a non-destructive evaluation technique based on electrical impedance tomography (EIT) can be effectively applied to image corrosion damage in materials. EIT uses electrostatic voltage and current measurements on the surface of a specimen to determine the conductivity distribution in the interior. In this paper, EIT is used to develop a method to determine material loss occurring on the inaccessible, or partially inacccessible portion $\gamma \subset \partial\Omega$ of the boundary $\partial\Omega$ of a material which occupies an open bounded domain $\Omega \subset R^2$ by measuring

*Corresponding author. Tel.: 00-44-113-2335181; Fax: 00-44-113-2335090;
E-mail: amt5ld@amsta.leeds.ac.uk
[1]On study leave.

ISSN 1068-2767 print: ISSN 1029-0281 online
DOI: 10.1080/10682760290007453

voltages and currents (Cauchy data) on a remaining (accessible) portion $\Gamma \subset \partial\Omega - \gamma$. Although it is not necessary that $\gamma \cup \Gamma = \partial\Omega$, we shall consider, for simplicity, only the case $\Gamma = \partial\Omega - \gamma$. The boundary $\partial\Omega$ is assumed to be smooth in the sense of Liapunov, see e.g. Kellogg (1953), such that Green's formula is applicable. Therefore, we consider the Laplace equation in a two-dimensional damaged or transformed finite plate Ω with, for example, corrosion or continuous steel casting, for the potential u, namely,

$$\nabla^2 u = 0, \quad \text{in } \Omega \tag{1}$$

subject to the boundary conditions

$$u = f, \quad \frac{\partial u}{\partial n} = g, \quad \text{on } \Gamma \tag{2}$$

$$\alpha u + \beta \frac{\partial u}{\partial n} = h, \quad \text{on } \gamma \tag{3}$$

where f, g, h, α and β are prescribed functions such that $\alpha\beta \geq 0$, $\alpha^2 + \beta^2 \neq 0$, and n is the outward normal to the boundary $\partial\Omega$.

Practically, we would require that the corroded part γ is a perfect conductor, i.e. $\alpha = 1$, $\beta = 0$, $h = 0$, or insulated, i.e. $\alpha = 0$, $\beta = 1$, $h = 0$. Non-linear boundary conditions on γ, which take into account the chemical reduction and oxidation occurring on the boundary, can also be considered, see Vogelius and Xu (1998). A more realistic, boundary inverse problem would include transient effects in which the Laplace Eq. (1) is replaced by the heat equation. This problem has been addressed by Bryan and Caudill (1996) where they dealt with periodic flux in an infinite strip where one of the boundaries of the strips was unknown.

In Eqs. (2) and (3), Γ and γ are, in general, two simple arcs having in common the endpoints only, and this problem occurs in several contexts such as corrosion detection by electrostatic measurements, see Kaup and Santosa (1995) and Kaup *et al.* (1996), and of planar crack detection in non-ferrous metals subject to electromagnetic measurements, see McIver (1991).

The uniqueness in determining γ in the problem (1)–(3) when $\alpha = 1$, $\beta = 0$ or $\alpha = 0$, $\beta = 1$, follows from the unique analytical continuation property for the Laplace equation, see Beretta and Vessella (1998). However, connected to this inverse problem, is the question of uniqueness when the more general Robin boundary condition (2) is prescribed on the unknown boundary γ, thus allowing convective corroded damage to occur, see Canuto *et al.* (2001). The second theoretical issue is stability. Unfortunately, our inverse problem is severely ill-posed, see Aparicio and Pidcock (1996), and we cannot expect good stability with the usual topologies, because an ill-posed Cauchy problem for the Laplace equation is involved. In fact, in Alessandrini (1997) it is shown that the most one can hope for is logarithmic continuous dependence of γ from the Cauchy data f and g. Further, in the ill-posed problem, stability can be restored based on additional information on the input and output data, see Beretta and Vessella (1998), Rondi (1999), Bukhgeim *et al.* (2000) and Cheng *et al.* (2001).

Prior to this study, numerical methods were devised for an insulated corroded material, i.e. zero Neumann condition $\alpha = 0$, $\beta = 1$, $h = 0$, see Aparicio and Pidcock (1996). They assumed the potential u to be monotonic along the unknown curve γ and presented two numerical methods for determining an insulated corroded boundary. The first one solves the problem in a closed form and was used to define a parameter that describes the ill-posedness of the problem. The effect of this parameter on a second method based on inverse mapping was thereafter investigated. Both methods reflected the ill-posedness of the problem but they did not produce stable solutions, in addition to the *a priori* assumption of the unknown $u_{|\gamma}$ being monotonic.

Recently, for a perfect conducting corroded material, i.e. zero Dirichlet conditon, $\alpha = 1$, $\beta = 0$, $h = 0$, which arises in the study of a convectively cooling continuously casting problem, see Siegel (1986), Hon and Wu (2000) approximated the solution $u(x, y)$ as a linear combination of harmonic functions and then determined a curve $Y = \{(x, y) \in \overline{\Omega} \mid u(x, y) = 0\}$. However, their solution was found to be highly unstable when noise was introduced in the input data f and g. Further, this method of solution does not seem easily extendable when the corroded part is insulated, as in such a situation one will have to determine a curve $Y \subset \overline{\Omega}$ on which $\partial u/\partial n \mid_Y = 0$ and this becomes complicated.

Therefore, the purpose of this paper is to develop a stable and robust numerical solution for the ill-posed problem (1)–(3). Either the electric voltage $f(\not\equiv$constant) or current flux $g(\not\equiv 0)$ can be prescribed on Γ in Eq. (2) with the other one being measured as additional information.

For the discretisation of the problem (1)–(3) it is particularly advantageous to use the boundary element method (BEM) since we are dealing with a boundary value problem and the discretisation of the boundary only is the essence of the BEM. Further, it reduces the dimensionality of the problem by one and, unlike the domain discretisation methods such as the Finite-Difference Method (FDM) or the Finite Element Method (FEM), it does not require any domain discretisation moving meshes for the identification of the unknown boundary γ. Moreover, in our boundary element formulation any type of boundary condition can be prescribed on γ which may include a Robin boundary condition (3). Also many types of (linear) operators such as ∇^2, ∇^4, $\nabla^2 - \partial/\partial t$, $\nabla^2 - \partial^2/\partial t^2$, etc., in any dimension can be considered. The inverse formulation in which the Cauchy data (2) is prescribed only on a subportion of $\Gamma_1 \subset \Gamma$ of non-zero measure with either u or $\partial u/\partial n$ being prescribed on $\Gamma - \Gamma_1$ can also be dealt with using the BEM. Finally, our analysis can also be easily adapted to the situation when Γ is a simple closed curve and γ is an insulated simple closed curve or a simple arc surrounded by Γ, in which case the problem is known as the inverse cavity problem, see Kassab *et al.* (1997), or the inverse crack problem, see Friedman and Vogelius (1989), Alessandrini (1993) and Alessandrini *et al.* (1995), and models the detection by electrostatic measurements of a cavity, crack, flaw, fault or fracture in a conductor. A more general class of the latter inverse problem formulation is the inverse conductivity problem, see for more details Isakov (1998) and Ki and Sheen (2000).

Once the problem (1)–(3) has been discretised using the BEM in order to obtain a stable numerical solution the resulting system of non-linear equations is solved by minimizing a first-order Tikhonov's functional subject to simple bounds on the unknown variables. This approach is similar to that of Peneau *et al.* (1994) who investigated a problem of isotherm shape identification using the FEM.

2. THE BOUNDARY ELEMENT REGULARIZATION METHOD

Using Green's formula for the Laplace Eq. (1) we obtain the following integral equation

$$\eta(p)u(p) = \int_{\partial\Omega}\left[G(p,p')\frac{\partial u}{\partial n}(p') - u(p')\frac{\partial G}{\partial n_{p'}}(p,p')\right]dS_{p'}, \quad p \in \overline{\Omega} \tag{4}$$

where $\eta(p)$ is a coefficient function which is equal to 1 if $p \in \Omega$ and $\hat{\theta}/(2\pi)$ if $p \in \partial\Omega$ and $\hat{\theta}$ is the angle between the two sides of the tangents at $\partial\Omega$ at p'; in particular $\hat{\theta} = \pi$ if p belongs to a point on a smooth portion of $\partial\Omega$. In Eq. (4), $G(p,p')$ is the fundamental solution for the Laplace Eq. (1) which in two-dimensions is given by $G(p,p') = -(1/2\pi)\ln|p-p'|$. Using the boundary data (2) we obtain from Eq. (4)

$$\begin{aligned}\eta(p)u(p) = &\int_{\Gamma}\left[G(p,p')g(p') - f(p')\frac{\partial G}{\partial n_{p'}}(p,p')\right]dS_{p'} \\ &+ \int_{\gamma}\left[G(p,p')\frac{\partial u}{\partial n}(p') - u(p')\frac{\partial G}{\partial n_{p'}}(p,p')\right]dS_{p'}, \quad p \in \overline{\Omega}\end{aligned} \tag{5}$$

As the above integral Eq. (5) cannot, in general, be solved analytically we discretise the boundary $\partial\Omega$ in a counterclockwise manner into a collection of K boundary elements, namely, $\partial\Omega \approx \cup_{j=1}^{K} S_j$, where S_j may be curves or straight lines. (In 3-D, curved surfaces or polygonal surfaces could be used.) In what follows, consider $S_j = [p_{j-1}, p_j]$ to be straight line segments. For simplicity, we also adopt a constant BEM approximation in which the unknowns u and $\partial u/\partial n$ are assumed constant over each boundary element S_j and take their values at the midpoints $\tilde{p}_j = (p_j + p_{j-1})/2$, namely,

$$\begin{aligned}u(p) &\equiv u(\tilde{p}_j) = u_j, \quad p \in [p_{j-1}, p_j], \\ \frac{\partial u}{\partial n}(p) &\equiv \frac{\partial u}{\partial n}(\tilde{p}_j) = u'_j, \quad p \in [p_{j-1}, p_j].\end{aligned} \tag{6}$$

Based on the BEM approximations (6), Eq. (5) becomes

$$\eta(p)u(p) = \sum_{j=1}^{N}[A_j(p)u'_j + B_j(p)u_j] + \sum_{j=N+1}^{M+N}[A_j(p)g_j + B_j(p)f_j], \quad p \in \overline{\Omega} \tag{7}$$

where $f_j = f(\tilde{p}_j)$, $g_j = g(\tilde{p}_j)$,

$$A_j(p) = \int_{S_j} G(p,p')\,dS_j(p'), \quad B_j(p) = -\int_{S_j}\frac{\partial G}{\partial n_{p'}}(p,p')\,dS_j(p') \tag{8}$$

M is the number of boundary elements on Γ, N is the number of boundary elements on γ, and thus $K = M + N$. Collocating Eq. (7) at the boundary nodes $\tilde{p}_i$ for $i = \overline{1,K}$, and Eq. (3) at the boundary nodes $\tilde{p}_i$ for $i = \overline{1,N}$, we obtain a system of $(K+N)$ equations,

namely,

$$\sum_{j=1}^{N}[A_{ij}u'_j + B_{ij}u_j] + \sum_{j=N+1}^{M+N}[A_{ij}g_j + B_{ij}f_j] = 0, \quad i = \overline{1, K} \tag{9}$$

$$\alpha_j u_j + \beta_j u'_j = h_j, \quad j = \overline{1, N} \tag{10}$$

where $\alpha_j = \alpha(\tilde{p}_j)$, $\beta_j = \beta(\tilde{p}_j)$, $h_j = h(\tilde{p}_j)$,

$$A_{ij} = \int_{S_j} G(\tilde{p}_i, p')\, dS_j(p'), \quad B_{ij} = -\int_{S_j} \frac{\partial G}{\partial n_{p'}}(\tilde{p}_i, p')\, dS_j(p') - \delta_{ij}\eta_j \tag{11}$$

$\eta_j = \eta(\tilde{p}_j)$ and δ_{ij} is the Kronecker delta tensor. For two-dimensional straight line elements, $S_j = [p_{j-1}, p_j]$ with endpoints $p_{j-1} = (x_{j-1}, y_{j-1})$ and $p_j = (x_j, y_j)$ the matrices A_{ij} and B_{ij} in (11) can be evaluated analytically resulting in

$$A_{ij} = (-a\cos(\phi)\ln(a/b) + h - h\ln(b) - a\psi\sin(\phi))/(2\pi) \tag{12}$$

$$B_{ij} = \begin{cases} -0.5, & \text{if } i = j \\ \operatorname{sgn}(\chi_{j-1} - \chi_j)\psi/(2\pi), & \text{if } i \neq j \text{ and } y_i \in (y_{j-1}, y_j) \\ \operatorname{sgn}(\chi_j - \chi_{j-1})\psi/(2\pi), & \text{if } i \neq j \text{ and } y_i \notin (y_{j-1}, y_j) \end{cases} \tag{13}$$

where χ_{j-1} and $\chi_j \in [0, \pi]$ are the angles between the positive x-axis and the straight lines $[\tilde{p}_i, p_{j-1}]$ and $[\tilde{p}_i, p_j]$ in the upper-half plane, respectively, and $h = \mid p_j - p_{j-1} \mid$, $a = \mid \tilde{p}_i - p_{j-1} \mid$, $b = \mid \tilde{p}_i - p_j \mid$, $\cos(\phi) = (a^2 + h^2 - b^2)/(2ah)$, $\sin(\phi) = (1 - \cos^2(\phi))^{1/2}$ and $\psi = \cos^{-1}((a^2 + b^2 - h^2)/(2ab))$. In Eq. (10), $\alpha_j^2 + \beta_j^2 \neq 0$ and we assume, for simplicity, that $\beta_j \neq 0$ and, in fact, take $\beta_j = 1$ for $j = \overline{1, N}$. Then introducing (10) into (9) we obtain a system of K equations, namely,

$$\sum_{j=1}^{N}[B_{ij} - \alpha_j A_{ij}]u_j + \sum_{j=1}^{N} A_{ij}h_j + \sum_{j=N+1}^{M+N}[A_{ij}g_j + B_{ij}f_j] = 0, \quad i = \overline{1, K} \tag{14}$$

For a given initial guess $p_1^{(0)}, \ldots, p_{N-1}^{(0)}$, we write the system of Eq. (14) as

$$\sum_{j=1}^{N}[B_{ij} - \alpha_j A_{ij}]u_j + \sum_{j=N+1}^{M+N} A_{ij}u'_j = -\sum_{j=1}^{N} A_{ij}h_j - \sum_{j=N+1}^{M+N} B_{ij}f_j, \quad i = \overline{1, K} \tag{15}$$

where we have replaced the measured flux data g_j with the control variable u'_j. Alternatively, we could have worked with the control variable u_j replacing f_j. Equation (15) is a linear system of K equations with K unknowns, namely, u_j for $j = \overline{1, N}$, and u'_j for $j = \overline{(N+1), K}$. Solving this system using for example a Gaussian elimination method we produce in particular the values of $u_j^{(c)}$ for $j = \overline{(N+1), K}$, where the

superscript (c) denotes the calculated value of the flux on the boundary Γ. We can then minimize the Tikhonov functional

$$\text{Objf}(p_1, \ldots, p_{N-1}) = \| \underline{u}'^{(c)} - \underline{g}^{\epsilon} \|^2 + \lambda \sum_{j=1}^{N} | p_j - p_{j-1} |^2 \tag{16}$$

where $\lambda > 0$ is a regularization parameter to be prescribed and $\underline{g}^{\epsilon}$ represents the noisy measurement data for the exact $\underline{g}$. The minimization of the functional (16) is performed using the NAG routine E04UCF, which is designed to minimize an arbitrary smooth function (which may include simple bounds on the variables, linear constraints and smooth non-linear constraints) using a sequential quadratic programming method, see Gill *et al.* (1986).

3. NUMERICAL RESULTS AND DISCUSSION

At this stage we observe that the objective functional (16) depends on $(2N-2)$ variables which are the coordinates (x_j, y_j) of the points p_j for $j = \overline{1,(N-1)}$, whilst only M additional data g_j, for $j = \overline{(N+1),(N+M)}$, of the flux on the boundary Γ are imposed. For the simplicity of the BEM implementation we take $M = N$, in order to make the minimization over-determined, or at least determined. In this section, we consider the case when the unknown boundary γ is the graph of an unknown function $y : [0, l] \to R$ taking the x-axis to pass through the endpoints $y(0) = y(l) = 0$ of γ and fixing the origin at $x = 0$. Thus the endpoints of the boundary elements S_j on γ will have the known equally-spaced x-coordinates $x_j = jl/N$ for $j = \overline{0, N}$. Further, since $y(0) = y(l) = 0$, the functional (16) will depend on only $(N-1)$ unknowns, $y_1, \ldots, y_{N-1}$, where $y_j = y(x_j)$. Then the functional (16) becomes of the form

$$\begin{aligned} \text{Objf}(y_1, \ldots, y_{N-1}) &= \| \underline{u}'^{(c)} - \underline{g}^{\epsilon} \|^2 + \lambda \| \underline{y}' \|^2 \\ &= \sum_{j=N+1}^{K} (u_j'^{(c)} - g_j^{\epsilon})^2 + \lambda [y_1^2 + y_{N-1}^2 + \sum_{j=2}^{N-1} (y_j - y_{j-1})^2] \end{aligned} \tag{17}$$

where we have stopped penalising the x-coordinates in the norms $| p_j - p_{j-1} |$ since they are known. It is worth noting that a zeroth-order regularization procedure based on penalising the norm of the solution $\| \underline{y} \|$, rather than its derivative $\| \underline{y}' \|$ did not produce sufficiently accurate and stable numerical results and this conclusion is consistent to that found by Peneau *et al.* (1994). So, the assumption of smoothness of the numerical solution for γ, as given by the Tikhonov first-order functional (17), is essential in obtaining an accurate and stable solution. Alternatively, instead of (17) one may parameterise the unknown boundary γ with various approximating functions and then the problem turns into a parameter estimation problem to determine the coefficients of the approximation, see Birginie *et al.* (1996).

We consider that the clean (undamaged) material at the time $t = 0$ of insertion into an engineering environment is a circle of radius 1, namely, $\Omega_0 = \{(x, y) \mid (x-1)^2 + y^2 < 1\}$, which may represent a circular plate or the cross-section of a long circular

cylindrical pipe. At the steady-state, as $t \to \infty$, the domain becomes corroded and degenerates into the damaged domain Ω. We assume that the upper semicircular part $\Gamma = \{(x, y) \mid (x-1)^2 + y^2 = 1, y \geq 0\}$ remains uncorroded and is known, whilst the corroded part $\gamma = \partial\Omega - \Gamma$ is totally, or partially unknown, but remains within the initial configuration Ω_0. Thus $l = 2$ and the simple bounds on the unknown variables are given by

$$-\frac{2}{N}[j(N-j)]^{1/2} < y_j < \frac{2}{N}[j(N-j)]^{1/2}, \quad j = \overline{1, (N-1)} \tag{18}$$

In order to illustrate a typical benchmark inversion we consider an insulated damaged material, i.e. $\alpha = 0$, $\beta = 1$, $h = 0$, and thus (15) simplifies as

$$\sum_{j=1}^{N} B_{ij} u_j + \sum_{j=N+1}^{M+N} A_{ij} u'_j = -\sum_{j=N+1}^{M+N} B_{ij} f_j, \quad i = \overline{1, K} \tag{19}$$

We consider the corroded damaged boundary γ given by the union of three portions γ_1, γ_2, γ_3, where

$$\begin{aligned} \gamma_1 &= \left\{(x, y) \mid \left(x - \tfrac{1}{4}\right)^2 + y^2 \leq \tfrac{1}{16}, y < 0\right\} \\ \gamma_2 &= \left\{(x, y) \mid (x-1)^2 + y^2 \leq \tfrac{1}{4}, y \geq 0\right\} \\ \gamma_3 &= \left\{(x, y) \mid \left(x - \tfrac{7}{4}\right)^2 + y^2 \leq \tfrac{1}{16}, y < 0\right\} \end{aligned} \tag{20}$$

This typical test example was chosen in order to ensure that $\gamma \subset \Omega_0$ is sufficiently complex and changes concavity, but any other graphs of continuous functions can be inverted. Further, γ given by Eq. (20) is a smooth curve in agreement with the minimization of (17) which imposes a first-order smoothness constraint on the solution. However, in Fig. 8 we have also tested another example involving the retrieval of a piecewise smooth continuous boundary.

The uniform BEM discretisation was obtained with $M = 40$ boundary elements on Γ, $N_1 = 10$ boundary elements on each of γ_1 and γ_3, and $N_2 = 20$ boundary elements on γ_2, such that $N = 2N_1 + N_2 = 40$. Further refinements in this mesh did not show any divergence of the numerical results and it was kept fixed in the inversion. We consider a non-constant voltage $f = x = \cos(\theta)$ prescribed on Γ, where $\theta \in [0, \pi]$ is the angular polar coordinate, for which, a direct problem solution, i.e. when γ is known, based on solving (19) using a Gaussian elimination method, gives rise to the non-zero current $g(\theta)$ on Γ shown in Fig. 1. From this figure it can be seen that the above mesh size is sufficiently fine for achieving very good accuracy. In order to simulate the inherent errors present in any practical experiment, the data g shown by ($\circ\circ\circ$) in Fig. 1 was then perturbed by $p \in \{1, 2, 3\}$ percent Gaussian normally distributed multiplicative random noise, $\underline{\epsilon}$, namely, $\underline{g}^{\epsilon} = \underline{g} + \underline{\epsilon}$, generated using the NAG routine G05DDF, with zero mean and standard deviation $\underline{\sigma} = (\sigma_i)_{i=\overline{(N+1), M}}$, where $\sigma_i = p \times \text{abs}(g_i)/100$. Additive random noise with zero mean and standard dev-

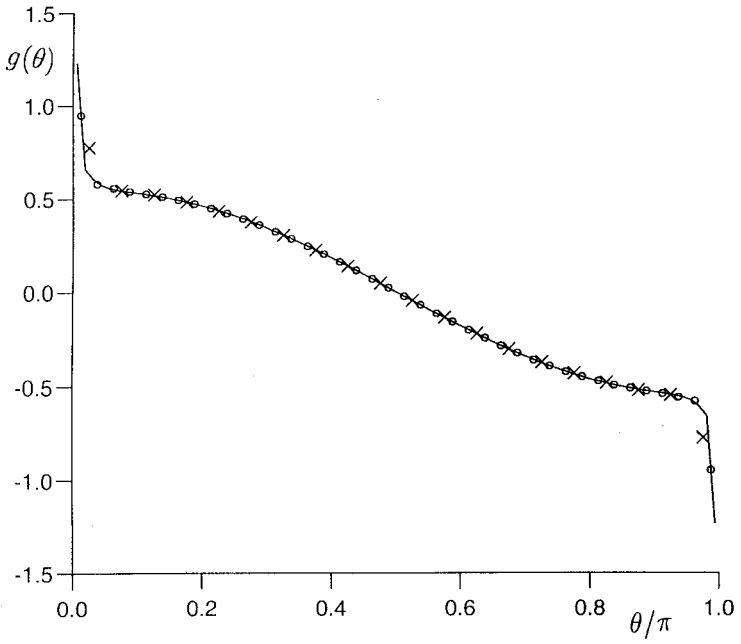

FIGURE 1 The values of the current $g(\theta)$ on Γ obtained for various BEM mesh discretisations, namely, ($\times \times \times$) $N_1 = 5$, $N_2 = 10$, $M = 20$; ($\circ \circ \circ$) $N_1 = 10$, $N_2 = 20$, $M = 40$ and (—) $N_1 = 20$, $N_2 = 40$, $M = 80$.

iation $\sigma = p \times \max\{\text{abs}(g_{|\Gamma})\}/100$ has also been tested and the same conclusions were obtained.

In the inverse analysis of retrieving the whole, or a portion of γ we have investigated three cases, namely:

Case 1 (γ_1, γ_3 known and γ_2 unknown) in order to investigate a simple shape γ_2 for which the number of measurements $M = 40$ is much larger than the number of unknowns $N_2 - 1 = 19$.
Case 2 (γ_2 known and γ_1, γ_3 unknown) in order to investigate the case when the unknown boundary is not simply-connected which violates the hypotheses of the theoretical studies mentioned in the introduction. In this case, the number of measurements is $M = 40$ and the number of unknowns is $2N_1 - 2 = 18$.
Case 3 (γ_1, γ_2, γ_3 all unknown) in order to investigate a complex shape $\gamma_1 \cup \gamma_2 \cup \gamma_3$ which changes concavity and for which the number of measurements $M = 40$ is comparable with the number of unknowns $2N_1 + N_2 - 1 = 39$.

The objective functional (17) has been minimized subject to the constraints (18) using the NAG routine E04UCF, with the gradient of Objf calculated using forward finite differences with a step of 10^{-3} which was found to be sufficiently small that a further decrease in this value does not affect significantly the accuracy of the numerical results. The initial guess was taken to be the constant 0.0, and the algorithm has been found to be robust as other initial guesses produced the same numerical convergent results. For example, for Case 1 and $p = 1$, the constant initial guesses -0.25, 0.0 and 0.25 produced the same convergent value for Objf $= 0.0014$, within 154, 127 and 124 iterations,

respectively, for $\lambda = 5 \times 10^{-3}$. In the functional (17), the choice of the regularization parameter $\lambda > 0$ is crucial for achieving the stability of the numerical solution, and in this study we have used an L-curve type criterion, see Hansen (1992), which plots on a log–log scale the least-squares gap $| \underline{u}'^{(c)} - \underline{g}^{\epsilon} |$ versus the norm of the derivative of the solution, $| \underline{y}' |$, for various values of λ. As with every practical method, the L-curve has its advantages and disadvantages. There are two main disadvantages or limitations of the L-curve criterion; understanding these limitations is the key to the proper use of the L-curve criterion and, hopefully, also to future improvements of the method. The first disadvantage is concerned with the reconstruction of very smooth exact solutions, see e.g. Tikhonov *et al.* (1998). For such solutions, Hanke (1996) showed that the L-curve criterion will fail, and the smoother the solution the worse the λ computed by the L-curve criterion. In fact, for $p = 0$, i.e. no noise, we have not obtained any L-curve. However, it is not clear how often very smooth solutions arise in applications and therefore in general $p > 0$. The second limitation of the L-curve criterion is related to its asymptotic behaviour as the problem size M increases. As pointed out by Vogel (1996), the regularization parameter λ computed by the L-curve criterion may not behave consistently with the optimal parameter λ_{opt} as M increases. However, this situation in which the same problem is discretised for increasing M, may not arise so often in practice. Usually the problem size M is fixed, such as $M = 40$ in our numerical investigation, by a particular measurement setup, and if a larger M is required then a new experiment must be performed. Apart from these limitations, the advantages of the L-curve criterion are its robustness and its ability to treat perturbations consisting of correlated noise, for more details see Hansen (2001).

Figures 2(a)–(c) show the L-curve plots for the Cases 1–3, respectively, for $p \in \{1, 2, 3\}$. The optimal values of λ are then chosen at the corners ('elbows') of these curves in order to balance the over-smooth regions, i.e. λ too large, and the under-smooth regions, i.e. λ too small. A more systematic way to find this elbow is to determine the maximum point of the curvature of the L-curve with respect to $\lambda > 0$, for more details see Hansen (1992, 2001) and Hansen and O'Leary (1993). This is confirmed in Figs. 3(a)–(c) which show the accuracy error-norms $| \underline{y} - \underline{y}^{(\text{exact})} |$, as functions of λ, for Cases 1–3, respectively, for $p \in \{1, 2, 3\}$. On comparing Figs. 2 and 3 it can be seen that as p increases, the elbow of the L-curve becomes broader and the error $| \underline{y} - \underline{y}^{(\text{exact})} |$ increases fairly dramatically as we move away from the optimal value for λ. However, this is to be expected since as the amount of noise p increases the inverse problem becomes more ill-posed and hence more difficult to solve. Of course in the absence of an exact solution $\underline{y}^{(\text{exact})}$ this is a rather heuristic argument, but then other more rigorous criteria such as the discrepancy principle, see Morozov (1966), or the generalized cross-validation, see Wahba (1977), can be adopted for comparison. In our study, Figs. 2(a)–(c) present clearly L-shaped curves and therefore the L-curve criterion is applicable. The optimal values λ_{opt} shown in Figs. 2(a)–(c) are then fixed in Figs. 4–7.

Figures 4(a)–(c) show the numerically retrieved boundaries obtained using the optimal values λ_{opt} shown in Fig. 2(c), for $p \in \{1, 2, 3\}$, in comparison with their exact targets in Cases 1, 2 and 3, respectively. From these figures it can be seen that in all the cases considered the numerical solutions are stable and consistent with the amount of noise p included in the input data g, and that they converge to their corresponding exact targets given by Eq. (20) as the amount of noise p decreases, i.e. as the data errors tend to zero, the numerical solution is convergent to the exact solution.

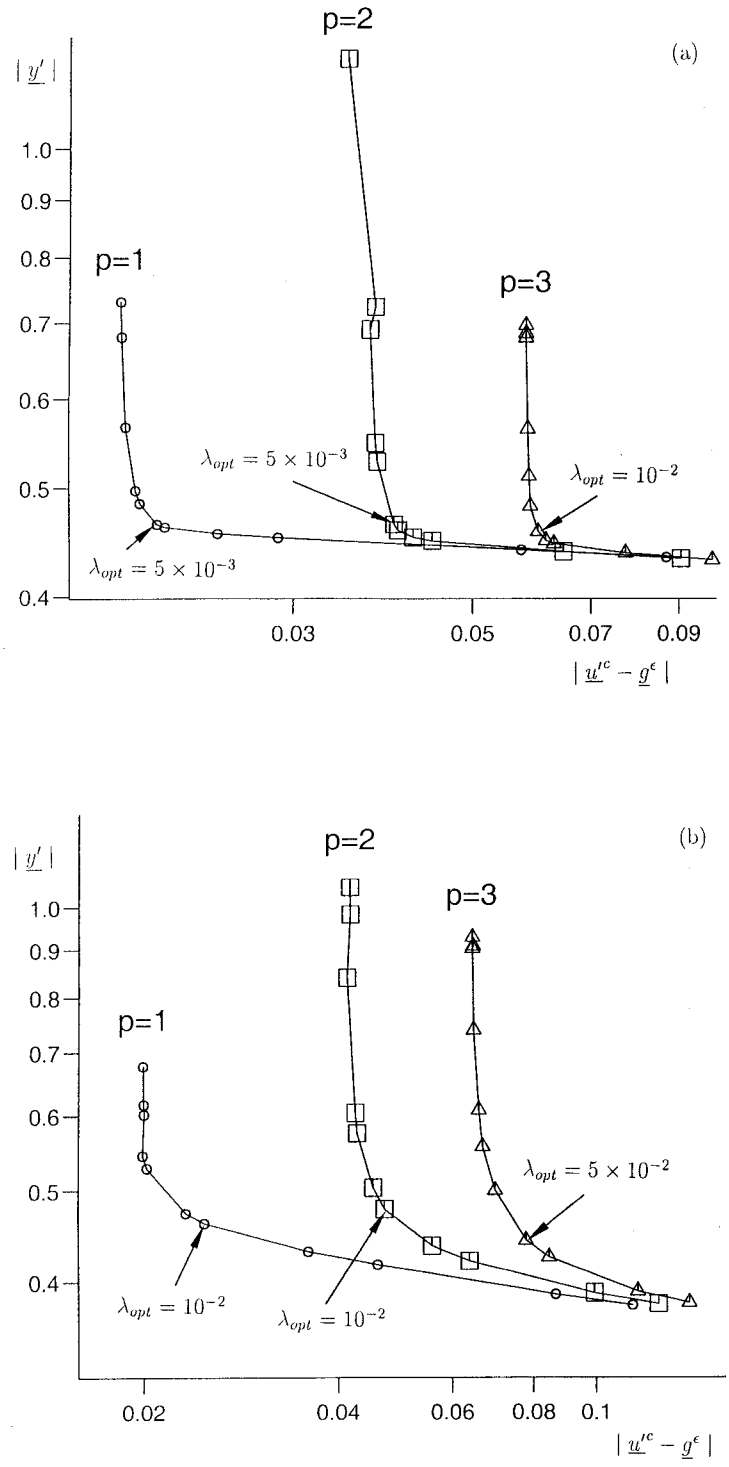

FIGURE 2 The L-curve plots of $|\underline{u}'^{c} - \underline{g}^{\epsilon}|$ versus the norm of the first-order derivative, $|\underline{y}'|$, for various values of $\lambda \in \{10^{-k}; k = \overline{0,5}\} \cup \{5 \times 10^{-k}; k = \overline{1,5}\}$ for $p \in \{1, 2, 3\}$ in (a) Case 1, (b) Case 2 and (c) Case 3.

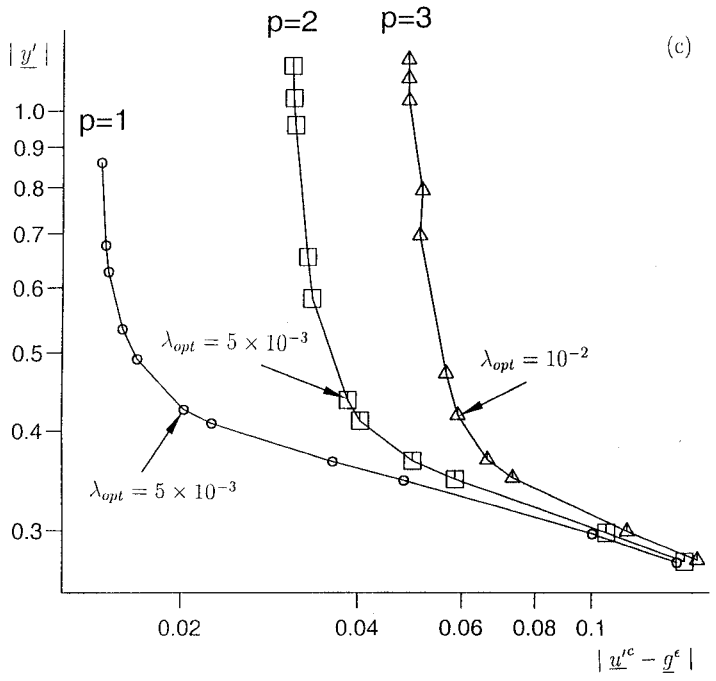

FIGURE 2 (Continued).

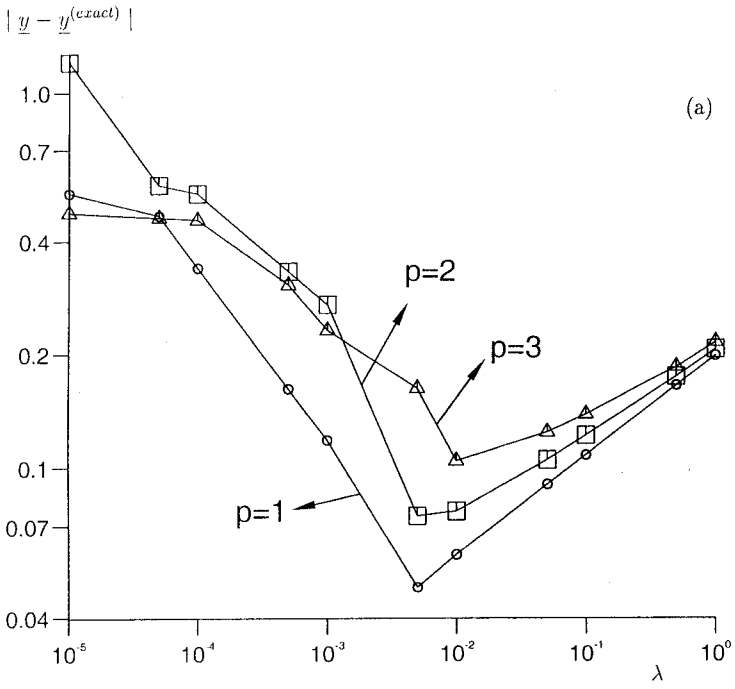

FIGURE 3 The accuracy error-norms $|\underline{y} - \underline{y}^{(\text{exact})}|$, as functions of λ, for $p \in \{1, 2, 3\}$ in (a) Case 1, (b) Case 2 and (c) Case 3.

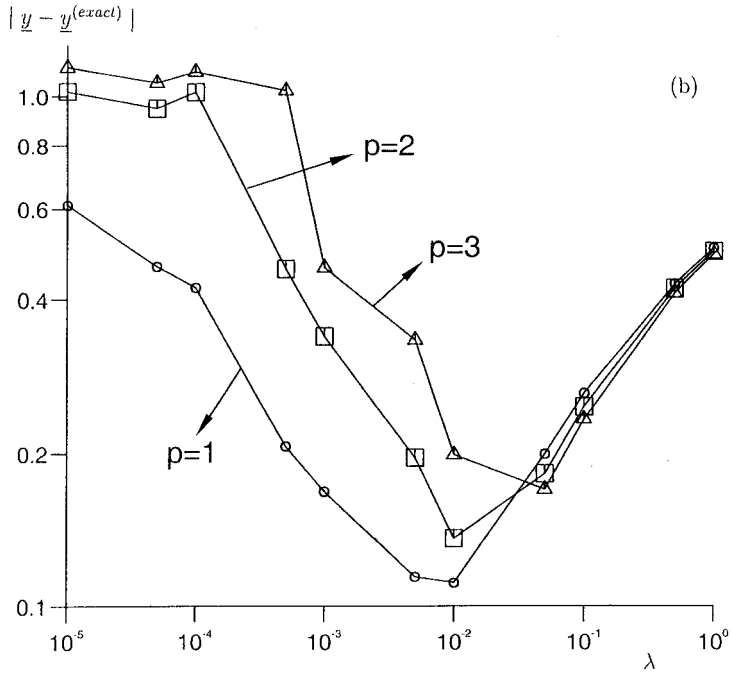

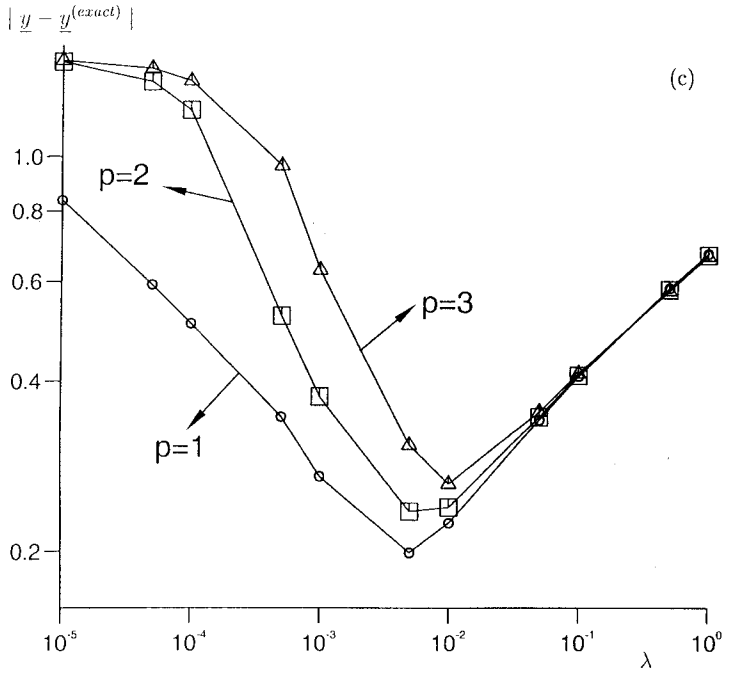

FIGURE 3 (Continued).

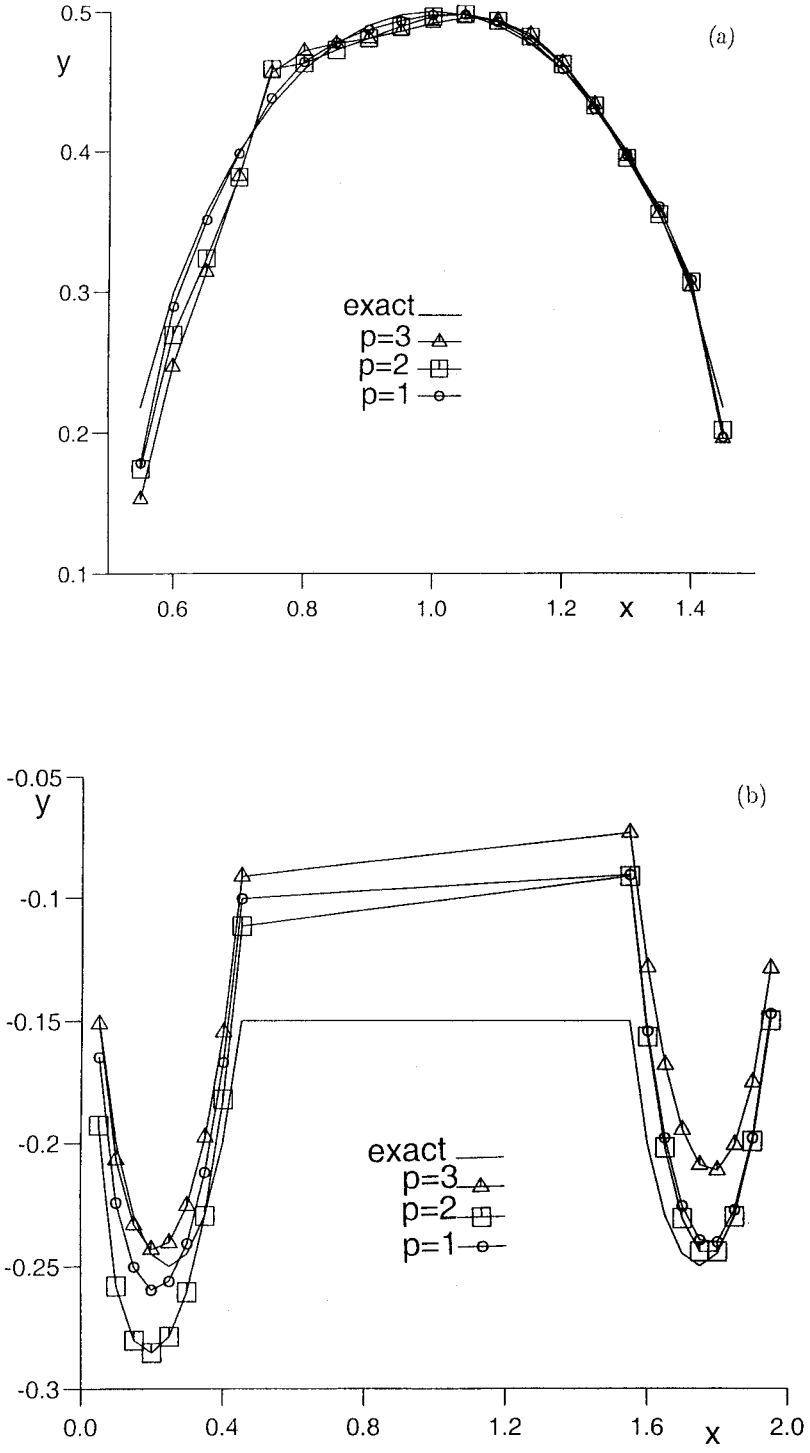

FIGURE 4 The numerically retrieved boundaries for $p \in \{1, 2, 3\}$ in comparison with their exact targets in (a) Case 1, (b) Case 2 and (c) Case 3.

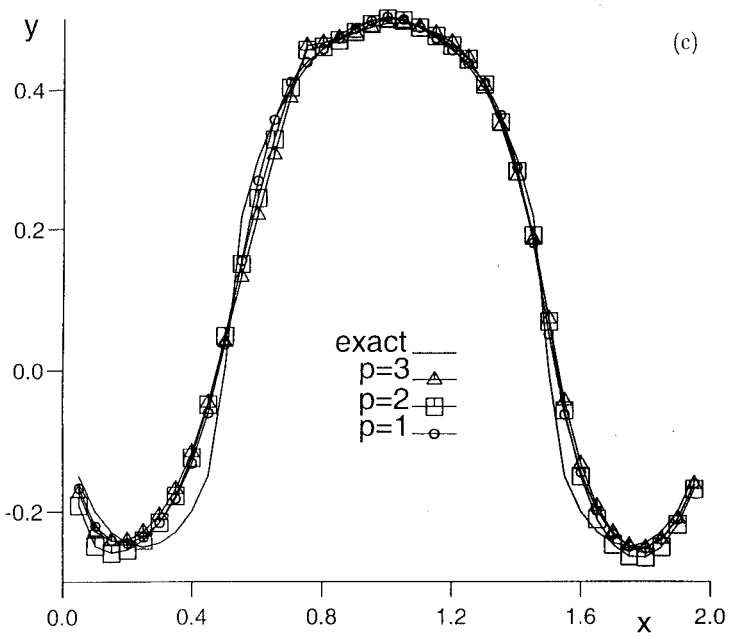

FIGURE 4 (Continued).

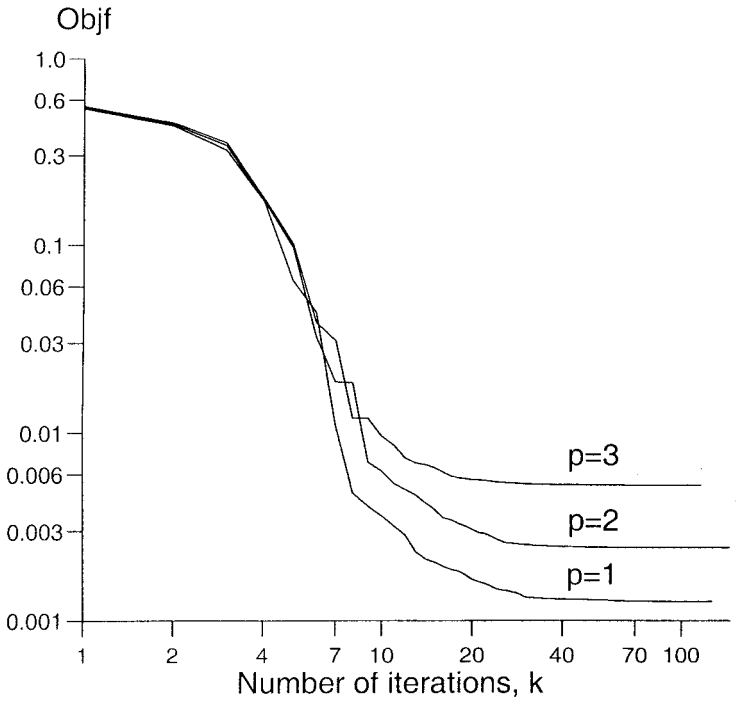

FIGURE 5 The convergence of the objective function Objf given by Eq. (17), as a function of the number of iterations, for $p \in \{1, 2, 3\}$ in Case 1.

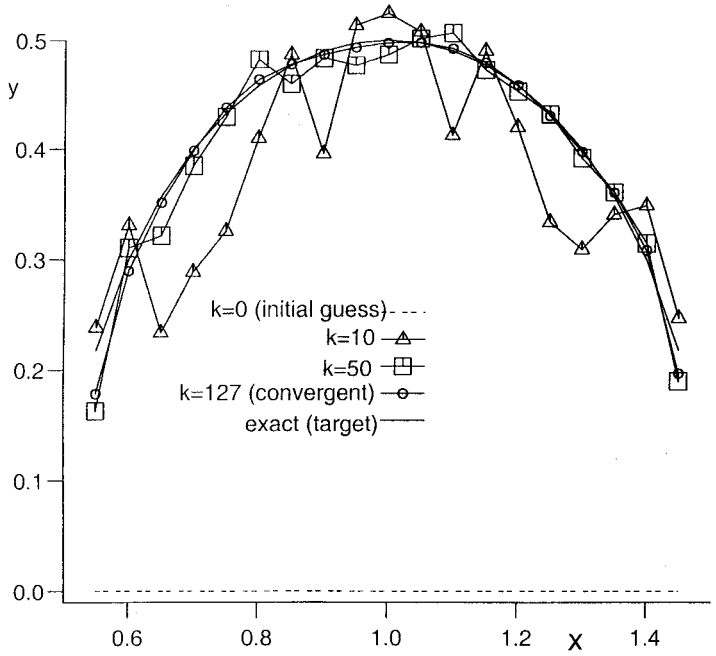

FIGURE 6 The convergence history of γ_2 for various numbers of iterations $k \in \{0, 10, 50, 127\}$, as the initial guess $\underline{y}^{(0)} = \underline{0}$ (dashed line), moves towards the semicircle target γ_2 in Case 1, for $p = 1$.

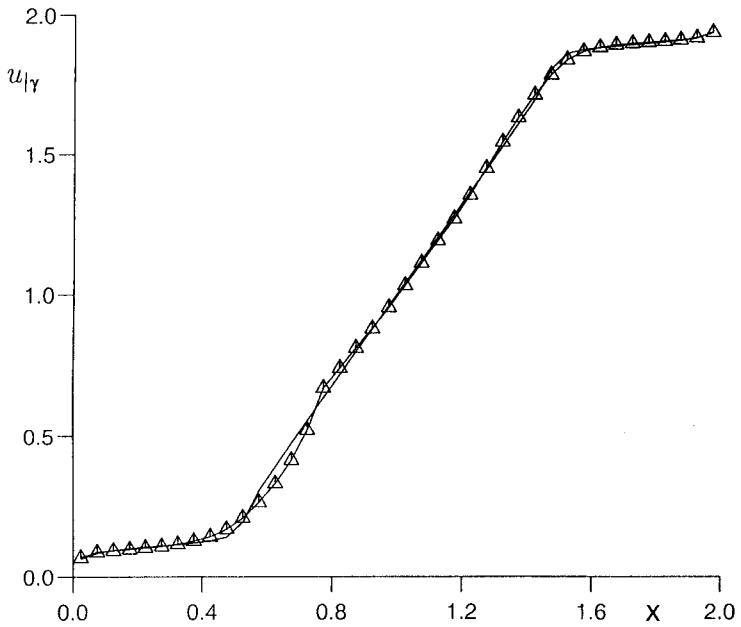

FIGURE 7 The numerical solution (–Δ–) for u on γ in comparison with the direct problem solution (—) in Case 3, for $p = 3$.

Figure 5 shows the monotonic decreasing convergence of the objective functional (17) which is minimized subject to the constraints (18), as a function of the number of iterations k, for various amounts of noise $p \in \{1, 2, 3\}$, for Case 1. From this figure it can be seen that the objective functional (17) levels off quickly after a small number (less than 30) of iterations. Although not illustrated it is reported that rate of convergence of Objf given by (17), is the fastest in Case 2, followed by Cases 1 and 3. This is to be expected since Case 3 contains the union of Cases 1 and 2, and because in Case 2 the unknown boundaries γ_1 and γ_3 are closer than in Case 1 to the known boundary Γ where the Cauchy data f and g are prescribed by Eq. (2). The convergence history of the iterative process in Case 1, for $p = 1$, is shown in Fig. 6. From this figure it can be seen that the unknown boundary γ_2 is detected reasonably accurately within 127 iterations with an l^2-error norm of 0.0481, see also Fig. 3(a), which is comparable with the amount of noise which is $\epsilon = 0.0248$ for this case. Further, it can be observed that after 10 iterations the numerical solution seems unstable, but it regularizes as the number of iterations increases and the process becomes convergent.

Figure 7 shows the numerical values for u on γ in Case 3 for $p = 3$, in comparison with the direct problem solution obtained by solving the direct problem using a Gaussian elimination method for inverting (19), when γ is taken as known. From Fig. 7 it can be seen that the numerical solution for $u|_\gamma$ is stable.

We have also investigated the situation when γ is piecewise–smooth by taking $\gamma_1 = [0, 0.5] \times \{0\}$ and $\gamma_3 = [1.5, 2] \times \{0\}$ and, as illustrated in Fig. 8 for Case 3, the same sound stability and good accuracy between the numerical solution and the analytical solution were obtained. In this figure, the optimal regularization parameters were chosen according to the L-curve criterion and were found to be $\lambda_{\text{opt}} = 5 \times 10^{-3}$ for

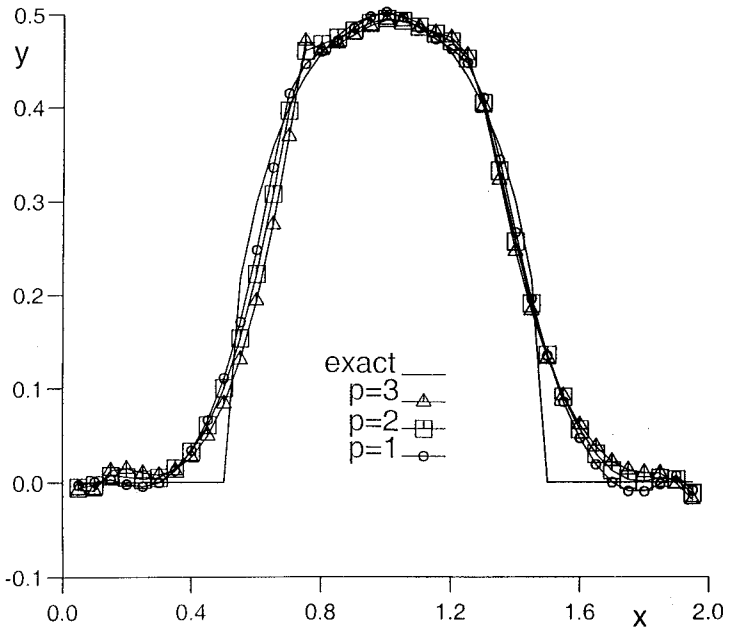

FIGURE 8 The numerically retrieved boundary for $p \in \{1, 2, 3\}$ in comparison with its exact piecewise smooth target $\gamma = ([0, 0.5] \times \{0\}) \cup \gamma_2 \cup ([1.5, 2] \times \{0\})$.

$p = 1$ and $\lambda_{\text{opt}} = 10^{-2}$ for $p \in \{2, 3\}$. The corner points $(0.5, 0)$ and $(1.5, 0)$ are, as expected, rounded-off since the minimization of the first-order regularization functional (17) imposes the numerical solution to be smooth.

Finally, although not illustrated it is reported that the numerical method proposed in this study was also obtained to be stable when solving the Dirichlet problem, i.e. $\alpha = 1$, $\beta = 0$, for all the Cases 1–3, for an analytical test function such as $u(x, y) = x^2 - y^2$.

4. CONCLUSIONS

In this paper, the inverse boundary determination in potential corroded damaged materials, which requires the determination of the location, size and shape of an unknown, or partially unknown, portion $\gamma \subset \partial\Omega$ of the boundary $\partial\Omega$ of a solution domain $\Omega \subset R^2$ in which Laplace's equation holds from additional Cauchy data on the remaining portion of the boundary $\Gamma = \partial\Omega - \gamma$, has been investigated numerically. This difficult inverse problem was approached using the BEM in conjunction with a Tikhonov first-order regularization procedure with the choice of the regularization parameter based on an L-curve type criterion, although alternatively the discrepancy principle may be equally used with the same performance. The constrained minimization procedure was found to be robust, independent on the initial guess, whilst the zeroth-order regularization was found to be significantly dependent on the initial guess. Several examples in which the unknown boundaries are represented by the graph of a function were thoroughly investigated and it was found that the proposed numerical method produces a stable approximate solution of the ill-posed problem concerning the retrieval of the unknown boundaries which is also convergent to the exact solution as the data errors tend to zero.

The boundary element regularization method proposed in this study can easily be extended to:

i) homogeneous anisotropic materials with conductivity given by the symmetric and positive definite (constant) tensor k_{ij} in which the EIT is governed by

$$\sum_{i,j} k_{ij} \frac{\partial^2 u}{\partial x_i \partial x_j} = 0, \tag{21}$$

ii) special inhomogeneous isotropic materials with conductivity $k(\underline{x}) > 0$ satisfying $\nabla^2(k^{1/2}(\underline{x})) + ck^{1/2}(\underline{x}) = 0$, in which the EIT is governed by

$$\nabla \cdot (k(\underline{x})\nabla u) = 0 \tag{22}$$

and is applied to a perfect conducting corroded part γ,

iii) non-linear isotropic materials with conductivity $k(u) > 0$ in which the EIT is governed by

$$\nabla \cdot (k(u)\nabla u) = 0 \tag{23}$$

and is applied to a perfect insulated corroded part γ. Furthermore, the BEM can be extended to three dimensions by using the fundamental solution $G(p,p') = 1/(4\pi \mid p - p' \mid)$ in the integral Eq. (4). In this case one could retrieve a Lipschitz continuous surface γ, see for more details the recent paper of Cheng *et al.* (2001) where logarithmic conditional stability estimates are given.

Further work will be concerned with extending the numerical method of this study to the retrieval of more complex boundaries which are not graphs of functions and also to include the transient effects.

Acknowledgements

The first author would like to acknowledge the Department of Mathematical and Computer Sciences at Colorado School of Mines since this research was performed there whilst on study leave from the University of Leeds.

NOMENCLATURE

A, B	coefficient matrices
G	fundamental solution of Laplace's equation
K	total number of boundary elements on $\partial\Omega$
M	number of boundary elements on Γ
N	number of boundary elements on γ
N_1	number of boundary elements on each of γ_1 and γ_3
N_2	number of boundary elements on γ_2
Objf	Tikhonov's first-order regularization objective functional
S_j	boundary elements
abs	absolute value (modulus)
f	electric voltage on Γ
g	current flux on Γ
h	prescribed function on γ
n	outward normal
p	percentage of noise
p_{j-1}, p_j	endpoints of S_j
$\tilde{p}_j$	midpoint of S_j
sgn	signum function
t	time
u	potential
(x, y)	Cartesian coordinates
(x_j, y_j)	Cartesian coordinates of p_j
Γ	known boundary where the Cauchy data is prescribed
Ω	solution domain
Ω_0	undamaged material at $t = 0$
$\partial\Omega$	boundary of Ω
α, β	constants, either 0 or 1, in general
γ	unknown, or partially unknown boundary
γ_1, γ_2, γ_3	portions of γ

δ_{ij}	Kronecker delta tensor
$\underline{\epsilon}$	Gaussian random variables
η	coefficient function
λ	regularization parameter
σ	standard deviation
θ	angular polar coordinate
$\hat{\theta}$	angle between the two sides of the tangents at $\partial\Omega$
$\|\|$	l^2-Euclidean norm of a vector

Superscripts

$'$	normal derivative
(c)	calculated (computed) value of the current flux on Γ
(exact)	exact solution for the unknown parametrised boundary γ
ϵ	perturbed data

Subscripts

opt	optimal value

References

Alessandrini, G. (1993). Stable determination of a crack from boundary measurements. *Proc. R. Soc. Edinburgh A*, **127**, 497–516.

Alessandrini, G., Beretta, E., Santosa, F. and Vessella, S. (1995). Stability in crack determination from electrostatic measurements at the boundary – a numerical investigation. *Inverse Probl.*, **11**, L17–24.

Alessandrini, G. (1997). Examples of instability in inverse boundary-value problems. *Inverse Probl.*, **13**, 887–897.

Aparicio, N.D. and Pidcock, M. (1996). The boundary inverse problem for the Laplace equation in two dimensions. *Inverse Probl.*, **12**, 565–577.

Beretta, E. and Vessella, S. (1998). Stable determination of boundaries from Cauchy data. *SIAM J. Math. Anal.*, **30**, 220–232.

Birginie, J.-M., Allard, F. and Kassab, A.J. (1996). Application of trigonometric boundary elements to heat and mass transfer problems. In: Brebbia, C.A., Martin, J.B., Aliabadi, M.H. and Haie, N. (Eds.), *BEM 18*, pp. 65–74. Braga, Portugal.

Bryan, K. and Caudill, L.F. Jr. (1996). An inverse problem in thermal imaging. *SIAM J. Appl. Math.*, **56**, 715–735.

Bukhgeim, A.L., Cheng, J. and Yamamoto, M. (2000). Conditional stability in an inverse problem of determining a non-smooth boundary. *J. Math. Anal. Appl.*, **242**, 57–74.

Canuto, B., Rosset, E. and Vessella, S. (2001). Quantitative estimates of unique continuation for parabolic equations and inverse initial-boundary value problems with unknown boundaries (*preprint*).

Cheng, J., Hon, Y.C. and Yamamoto, M. (2001). Conditional stability estimation for an inverse boundary problem with non-smooth boundary in R^3. *Trans. Am. Math. Soc.*, **353**, 4123–4138.

Friedman, A. and Vogelius, M. (1989). Determining cracks by boundary measurements. *Indiana Math. J.*, **38**, 527–556.

Gill, P.E., Hammarling, S., Murray, W., Saunders, M.A. and Wright, M.H. (1986). User's guide for LSSOL (Version 1.0). *Report SOL 86-1*. Department of Operations Research, Stanford Univ.

Hanke, M. (1996). Limitations of the L-curve method in ill-posed problems. *BIT*, **36**, 287–301.

Hansen, P.C. (1992). Analysis of discrete ill-posed problems by means of the L-curve. *SIAM Rev.*, **34**, 561–580.

Hansen, P.C. and O'Leary, D.P. (1993). The use of the L-curve in the regularization of discrete ill-posed problems. *SIAM J. Sci. Comput.*, **14**, 1487–1503.

Hansen, P.C. (2001). The L-curve and its use in the numerical treatment of inverse problems. In: Johnston, P. (Ed.), *Computational Inverse Problems in Electrocardiology*, pp. 119–142. WIT Press, Southampton.

Hon, Y.C. and Wu, Z. (2000). A numerical computation for inverse boundary determination problem. *Eng. Anal. Boundary Elem.*, **24**, 599–606.

Isakov, V. (1998). *Inverse Problems for Partial Differential Equations*. Springer-Verlag, Berlin.
Kassab, A.J., Hsieh, C.K. and Pollard, J. (1997). Solution of the inverse geometric problem for the detection of subsurface cavities by the IR-CAT method. In: Ingham, D.B. and Wrobel, L.C. (Eds.), *Boundary Integral Formulations for Inverse Analysis*, pp. 33–65. Comput. Mech. Publ., Southampton.
Kaup, P. and Santosa, F. (1995). Nondestructive evaluation of corrosion damage using electrostatic boundary measurements. *J. Nondestruct. Eval.*, **14**, 127–136.
Kaup, P., Santosa, F. and Vogelius, M. (1996). Method for imaging corrosion damage in thin plates from electrostatic measurements. *Inverse Probl.*, **12**, 279–293.
Kellogg, O.D. (1953). *Foundations of Potential Theory*. Dover Publ., New York.
Ki, H. and Sheen, D. (2000). Numerical inversion of discontinuous conductivities. *Inverse Probl.*, **16**, 33–47.
Morozov, V.A. (1966). On the solution of functional equations by the method of regularization. *Soviet Math. Dokl.*, **7**, 414–417.
McIver, M. (1991). An inverse problem in electromagnetic crack detection. *IMA J. Appl. Math.*, **47**, 127–145.
Peneau, S., Jarny, Y. and Sarda, A. (1994). Isotherm shape identification for a two dimensional heat conduction problem. In: Bui, H.D., Tanaka, M., Bonnet, M., Maigre, H., Luzzato, E. and Reynier, M. (Eds.), *Inverse Problems in Engineering Mechanics*, pp. 47–53. Balkema, Rotterdam.
Rondi, L. (1999). Optimal stability estimates for the determination of defects by electrostatic measurements. *Inverse Probl.*, **15**, 1193–1212.
Siegel, R. (1986). Boundary perturbation method for free boundary problem in convectively cooled continuous casting. *Trans. ASME. Sec. C*, **108**(1), 230–235.
Tikhonov, A.N., Leonov, A.S. and Yagola, A.G. (1998). *Nonlinear Ill-Posed Problems*, Vol. 1. Chapman & Hall, London.
Vogel, C.R. (1996). Non-convergence of the L-curve regularization parameter method. *Inverse Probl.*, **12**, 535–547.
Vogelius, M. and Xu, J. (1998). A nonlinear elliptic boundary value problem related to corrosion modeling. *Q. Appl. Math.*, **56**, 479–505.
Wahba, G. (1977). Practical approximate solutionto linear operator equations when the data is noisy. *SIAM J. Numer. Anal.*, **14**, 651–667.